Available online at www.sciencedirect.com
SCIENCE DIRECT®
Chemical Physics Letters 375 (2003) 253–260
CHEMICAL PHYSICS LETTERS
www.elsevier.com/locate/cplett

Intramolecular quantum chaos in doped helium nanodroplets

E. Polyakova [a], D. Stolyarov [a], X. Zhang [a], V.V. Kresin [b], C. Wittig [a,*]

[a] Department of Chemistry, University of Southern California, Los Angeles, CA 90089, USA
[b] Department of Physics, University of Southern California, Los Angeles, CA 90089, USA

Received 4 October 2002; in final form 8 April 2003
Published online 16 June 2003

Abstract

A mass spectrometric depletion spectrum (17 700–18 300 cm^{-1}) is reported for NO_2 in superfluid (0.37 K) helium nanodroplets. Gas phase NO_2 is believed to be vibronically chaotic at these energies. Transitions are broadened and blue-shifted relative to their gas phase counterparts. The spectrum is fitted reasonably well by setting all of the widths and shifts equal to 7 cm^{-1}. Modest dispersions (i.e., 90% lie within 2 cm^{-1} of the central values) are consistent with quantum chaos in NO_2. Relaxation is dominated by interactions of NO_2 with its non-superfluid helium nearest neighbors.

1. Introduction

Superfluid helium nanodroplets (hereafter referred to as He_n, where n is the number of He atoms) provide convenient environments for carrying out detailed studies of embedded molecules and aggregates under well-characterized, ultracold (0.37 K) conditions [1–3]. Research in this area has flourished following the seminal experiments of Vilesov, Toennies, and coworkers, in which molecular-level manifestations of He_n superfluidity were revealed in a series of elegant spectroscopic studies [4–7], and several exciting directions have been identified [8–10].

At this point in time, a significant number of fundamental and overtone vibrations of molecules and weakly bound complexes in their ground potential energy surfaces (PESs) have been examined [11–13]. In addition, molecular electronic spectra have revealed phonon wings, including a 'roton gap', radiationless decay, and details of the dopant–He_n interactions [14–18]. These studies have been carried out mainly in the regime of regular nuclear dynamics, where the goodness of vibrational quantum numbers is high. On the other hand, vibrational congestion, which often goes hand-in-hand with complex dynamics, has been noted in electronic spectra of large molecules, e.g., tetracene and pentacene [15,16]. However, in systems of such high dimensionality (i.e., having 84 and 108 vibrational degrees of freedom, respectively), state-resolved studies in the regime of chaotic dynamics are not feasible.

This article reports the first spectroscopic observations – *in a regime where the intramolecular*

* Corresponding author. Fax: 1-213-746-4945.
E-mail address: wittig@usc.edu (C. Wittig).

0009-2614/03/$ - see front matter © 2003 Elsevier Science B.V. All rights reserved.
doi:10.1016/S0009-2614(03)00714-0

dynamics are believed to be chaotic – of a small molecule embedded in superfluid helium nanodroplets. Chaotic and regular dynamical regimes differ qualitatively, and quantum-chaotic dynamics of the molecule under consideration (NO_2) has been implicated throughout the energy range of interest [19].

In the study reported here, the chaotic system is coupled weakly to an exceptionally well-characterized bath. The ultracold He_n host is used *to probe the dopant* by introducing two observables that are expected to provide signatures in and near the regime of quantum chaos: spectral shifts and widths.

It is advantageous that a great deal is known about NO_2. Strong mixing of the A^2B_2 and X^2A_1 states above the conical intersection of these PESs, due to breakdown of the Born–Oppenheimer approximation, yields A_1 and B_2 vibronic species, whose only means of communication in collision-free environments is rotation [20,21]. Each of these vibronic manifolds is believed to be quantum chaotic, e.g., for a given set of good quantum numbers (J and M_J) the nearest neighbor spacings follow a Wigner distribution [22]. Because NO_2 is small, its eigenstates are widely separated, i.e., they are $\sim$10 cm^{-1} apart on average for each vibronic manifold at $E \sim 18\,000$ cm^{-1}.

Thus, NO_2 is a good candidate for carrying out state-to-state studies of a chaotic molecular system embedded in He_n, inviting several questions: Will there be a correspondence between the respective line positions and intensities in the He_n and gas phase environments? What will be the shifts of the center frequencies relative to the gas phase values, and what is to be expected for the magnitudes and distributions of the decay widths associated with deactivation by the helium? What are the implications for photochemical studies? And so on.

It will be shown below that absorption lines are readily identified and related to their gas phase counterparts. With the current, admittedly modest, signal-to-noise ratio (S/N), the spectra can be fitted surprisingly well by blue-shifting all of the gas phase R_0 line positions by 7 cm^{-1}, adding 7 cm^{-1} widths to all of the lines, and adjusting the peak intensities to fit the spectrum. Fits obtained by fine-tuning the individual shifts and widths indicate modest dispersions around the central values. It is suggested that the results can be understood by consideration of the couplings that arise from the He_n perturber acting on the states of NO_2.

2. Theoretical considerations

Assume that the helium that surrounds embedded NO_2 acts as a perturbation to the gas phase molecule, and consider matrix elements that account for mixing, shifting, and deactivation of the NO_2 levels. Leaving aside rotation, which plays a secondary role, each of the NO_2 vibronic levels can be expanded in a basis of the vibrational levels of the A^2B_2 excited and X^2A_1 ground PESs, with the αth wavefunction given by:

$$\psi^{\alpha} = \sum_j C_j^{\alpha} \psi_e^{\mathrm{A}} \varphi_j^{\mathrm{A}} + \sum_k C_k^{\alpha} \psi_e^{\mathrm{X}} \varphi_k^{\mathrm{X}}, \tag{1}$$

where the summations, with indices j and k, are over the A^2B_2 and X^2A_1 vibrational levels, respectively; ψ_e^{A} is the A^2B_2 electronic wave function; φ_j^{A} is the jth vibrational wavefunction of the A^2B_2 PES; and C_j^{α} is the expansion coefficient for the jth vibrational level of the A^2B_2 PES. Likewise, ψ_e^{X} is the X^2A_1 electronic wavefunction, etc. The A^2B_2 part of ψ^{α} is much smaller than the X^2A_1 part, as is always the case for internal conversion [23].

Now consider perturbations of the NO_2 states, with explicit helium excitations suppressed; deactivation will be discussed below. The matrix elements of the perturbation brought about by the surrounding helium, V, is expressed as:

$$V_{\alpha\beta} = \left\langle \sum_j C_j^{\alpha} \psi_e^{\mathrm{A}} \varphi_j^{\mathrm{A}} + \sum_k C_k^{\alpha} \psi_e^{\mathrm{X}} \varphi_k^{\mathrm{X}} | V | \times \sum_{j'} C_{j'}^{\beta} \psi_e^{\mathrm{A}} \varphi_{j'}^{\mathrm{A}} + \sum_{k'} C_{k'}^{\beta} \psi_e^{\mathrm{X}} \varphi_{k'}^{\mathrm{X}} \right\rangle. \tag{2}$$

The randomness of the expansion coefficients results in small off-diagonal matrix elements due to cancellation, upon summation, of terms with $\alpha \neq \beta$. The degree of cancellation depends on the extent to which the levels are thorough mixtures of

a separable Hamiltonian basis [24]. For example, in the limit of complete cancellation, the surviving matrix elements are diagonal:

$$V_{\alpha\alpha} = \sum_j |C_j^\alpha|^2 V_{jj} + \sum_k |C_k^\alpha|^2 V_{kk}, \quad (3)$$

where $V_{jj} = \langle \varphi_j^A | V | \varphi_j^A \rangle$ and likewise for V_{kk}. It is assumed that V does not couple zeroth-order A^2B_2 and X^2A_1 levels. The V_{jj} and V_{kk} are the same for all of the ψ^α; only the expansion coefficients change from one level to the next.

According to Eqs. (1)–(3), for a modest energy interval, such as the one studied here (17 700–18 300 cm^{-1}) the energy levels will all be shifted relative to their gas phase values by comparable amounts when the mixing is thorough. This differs from the regime of regular dynamics, where shifts are mode-specific. In other words, the chaotic nature of the ψ^α levels results in vibrational averaging that leads to modest dispersion about the mean of the distribution of shifts. A similar conclusion is reached with the widths: the randomness of the expansion coefficients results in the different ψ^α levels having comparable decay widths.

The above considerations are intended to provide qualitative guidance; a detailed treatment will be presented in a full paper.

3. Experimental methods and results

The most relevant experimental parameters are indicated schematically in Fig. 1. There are three separately pumped chambers. In the first, He_n droplets are produced by expanding ultrapure helium (99.9999%, Spectra Gases) through a 5 μm diameter hole (National Aperture) that is cooled by using two closed-cycle helium refrigerators (CTI Cryogenics), one of which pre-cools the helium before it enters the nozzle assembly. For the work reported here, the stagnation temperature was 14.5 K and the pressure was 40 bar. The mean size of the clusters produced under these conditions is $\langle n \rangle \sim 9000$ [25]. Temperatures were measured with a Si diode sensor (Lakeshore ±0.1 K). The source chamber operating pressure is 2×10^{-4} mbar.

After passing through a 400 μm diameter skimmer, the droplet beam passes through a 3 cm long pickup cell containing NO_2 (Matheson, 99.5%, used without purification) that is 10 cm downstream from the nozzle. The background pressure (Granville-Phillips gauge) of the second chamber was $\sim10^{-7}$ mbar, and the largest signals were recorded with 4×10^{-7} mbar.

The detection region is separated from the pickup chamber by a 5 mm diameter aperture that

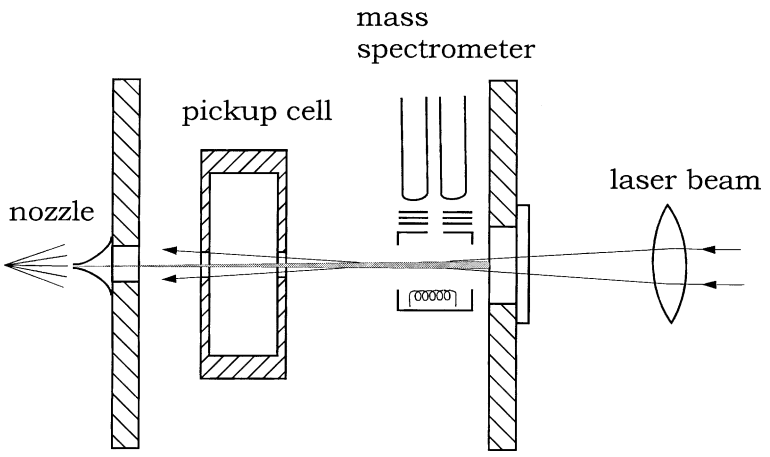

Fig. 1. Experimental arrangement (not to scale). The source, pickup, and detection chambers are pumped separately. The nozzle is at 14.5 K, and the He pressure behind the nozzle is 40 bar. The laser beam is brought to a focus in the detection chamber to avoid damaging the nozzle.

is 12 cm from the exit of the pickup cell. The background pressure in the detection chamber is $\sim 10^{-8}$ mbar. The use of turbomolecular pumps in the second and third chambers minimizes problems that arise from contamination by impurities. A quadrupole mass spectrometer (Balzers) was used to monitor the depletion of signals arising from droplets containing NO_2. The absorption of laser radiation results in the evaporation of He atoms from the droplets, each atom requiring ~ 5 cm^{-1} for evaporation. Thus, ~ 3600 He atoms are evaporated following the absorption of an 18 000 cm^{-1} photon. This shrinkage results in less efficient electron impact ionization of those clusters that have absorbed a photon, and consequently have a smaller cross-section. This is the basis of the mass spectrometer depletion spectrum. The largest depletions observed in the present study were $\sim 7\%$ (Fig. 2). The spectrum shown in Fig. 2 was obtained by monitoring $m/e = 30$. No significant differences were observed when monitoring different m/e peaks, i.e., 46 (NO_2^+), 30 (NO^+), and 8 (He_2^+).

The mass spectrometer was installed with its quadrupole axis perpendicular to the molecular beam axis so the laser beam could be overlapped with the molecular beam. The length of this interaction region is ~ 75 cm, corresponding to a duration of the depletion signal of ~ 2.5 ms. The electron multiplier output of the mass spectro-

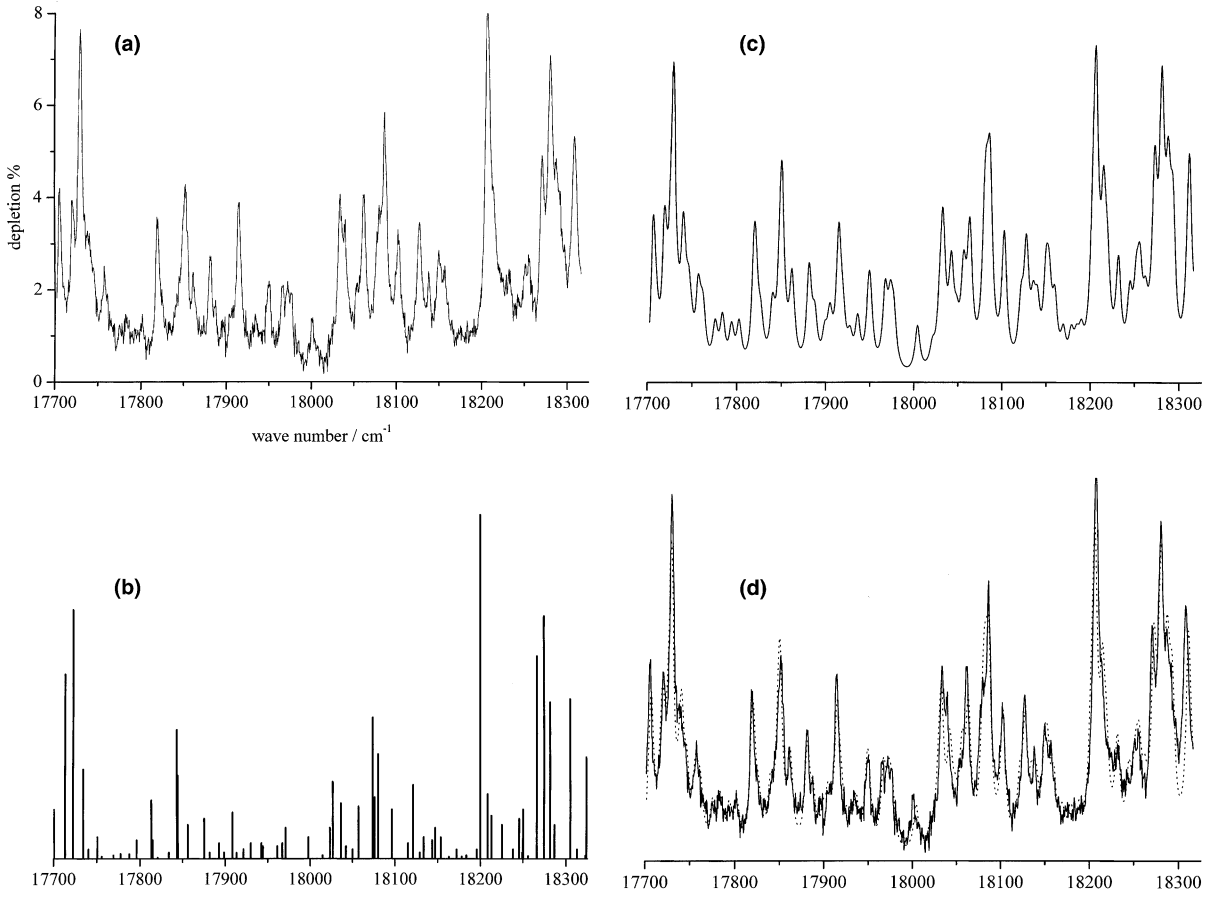

Fig. 2. (a) Mass spectrometer depletion spectrum. (b) Frequencies and intensities of R_0 lines recorded by using LIF are taken from Georges et al. [22]. (c) All of the lines in (b) have been assigned 7 cm^{-1} widths and blue-shifted by 7 cm^{-1}. The intensities are fitted to the experimental spectrum. (d) The experimental and simulated spectra are overlapped.

meter was connected directly to a 12-bit ADC computer board (Gage Applied Sciences, CS8012).

A dye laser (Continuum ND6000, Fluorescein 548 dye) was pumped by the second harmonic of a Nd–YAG laser (Continuum, Powerlite 7020), yielding radiation in the region 546–565 nm. High energy pulses (40 mJ) were used, because of the small NO_2 absorption cross-sections (i.e., $\sim 10^{-19}$ cm^2 for the corresponding gas phase transitions [26]). Note that N_2O_4 does not absorb in this spectral region, making spectral signatures insensitive to the pickup of a second NO_2 by a cluster already containing one NO_2. To avoid damaging the nozzle, a 50 cm focal length lens was used. Calibration of the laser frequency was carried out by simultaneously recording opto-galvanic spectra with a commercial hollow cathode Al–Ne discharge lamp, as described elsewhere [27].

Fig. 2a shows the experimental spectrum. The scan used a step size of 0.6 cm^{-1}, with a 0.08 cm^{-1} laser linewidth; 1000 points were recorded. This large step size was deemed appropriate after many scans over smaller frequency intervals, using smaller step sizes, revealed the large linewidths shown in Fig. 2a. Each point averages the results from 3000 laser pulses; approximately 50 h was required to record the spectrum. Fig. 2b shows the R_0 lines recorded by Georges et al. [22] by using LIF, and in Fig. 2c each of these lines has been assigned a 7 cm^{-1} width, the entire spectrum has been blue-shifted by 7 cm^{-1}, and the peak heights have been adjusted to fit the experimental spectrum. Fig. 2d shows an overlay of (a) and (c).

Varying all of the widths and center frequencies independently provides, of course, excellent fits. Though not unique, they indicate that the dispersions of the distributions of shifts and widths around their central values are modest. For example, 90% of the shifts and widths thus obtained lie within 2 cm^{-1} of the central values. More quantitative information about the dispersions will be forthcoming when higher quality spectra are available.

To our surprise, we were unable to find a literature report of a uv/visible spectrum of NO_2 recorded under matrix isolation conditions. Thus, an experiment was carried out in which Ne atoms were added to embedded NO_2. Even a single Ne atom obliterated the structure shown in Fig. 2, resulting in continuous absorption. This underscores the importance of the weak, homogeneous helium matrix.

4. Discussion

A noteworthy aspect of the spectrum presented here is that the shifts and widths do not differ significantly from line to line. Namely, the region 17 700–18 300 cm^{-1} can be fitted reasonably well by using the gas phase line positions and a 7 cm^{-1} blue-shift and a 7 cm^{-1} width. Because intramolecular coupling in NO_2 is *strong*, whereas the coupling of NO_2 to the helium is relatively *weak*, the shifts and widths can be understood on the basis of the model described by Eqs. (1)–(3). In this section, we: (i) argue against effects other than relaxation as the main origin of the widths; (ii) point out an important earlier paper that is germane to the work discussed here; and (iii) comment on the mechanism and model.

4.1. Origin of the widths

The saturation of allowed electric dipole transitions of gaseous molecular absorbers is encountered frequently in experiments that use pulsed laser radiation [20]. Because of the large laser energies used here (i.e., 40 mJ), effects that might accompany efficient optical excitation must be considered. Specifically, can they account for widths of ~ 7 cm^{-1}?

A useful figure-of-merit is the product $\sigma_{abs}\Phi$, where σ_{abs} is the photon absorption cross section and Φ is the fluence [28]. Saturation occurs when $\sigma_{abs}\Phi$ is comparable to or exceeds unity. For example, with $\sigma_{abs} \sim 10^{-19}$ cm^2, which is characteristic of gas phase NO_2 transitions [26], $\Phi \sim 10^{19}$ photons cm^{-2} will result in saturation. Absorption cross-sections of gaseous species are usually reported as empirical parameters that are valid for a given instrumental resolution, often with a measurement linewidth that exceeds the linewidth of the absorber. The estimate of $\sigma_{abs} \sim 10^{-19}$ cm^2 is conservative in light of the fact that our 0.08 cm^{-1} laser linewidth is significantly larger than the

widths due to spontaneous emission and Doppler broadening. Because the pulses used in our experiment contain approximately 10^{17} photons, saturation should be considered for laser beam diameters comparable to, and smaller than, ~1 mm, which occurs in the focal region (Fig. 1).

Saturation broadening of NO_2 transitions cannot, by itself, be responsible for the linewidths, because this would require $\sigma_{abs}\Phi$ values of $\sim 10^4$ [29], which is unreasonably large. For example, for a σ_{abs} value of 10^{-19} cm^2, Φ would have to be $\sim 10^{23}$ photons cm^{-2}, and beam diameters smaller than ~10 μm would be required. Even then, saturation would occur only over a small fraction of the region where the laser and molecular beams overlap, i.e., near the focal region indicated in Fig. 1.

Photoexcitation followed by relaxation heats the cluster, resulting in evaporation, with the cluster temperature in excess of 0.37 K for the remainder of the laser pulse, as demonstrated by Vilesov and co-workers [15]. For large clusters, the mass spectrometer ionization cross-section is proportional to the geometric cross-section [25], which varies as $n^{2/3}$. In this regime, the one-photon depletion signal for a given cluster size is given by:

$$I_{\mathrm{depl}} = 1 - [1 - 3600/n]^{2/3}, \quad n > 3600 \tag{4a}$$

$$= 1, \quad n \leqslant 3600, \tag{4b}$$

where it is assumed that the absorption of an 18 000 cm^{-1} photon results in the evaporation of 3600 He atoms. Eqs. (4a) and (4b) must be averaged over the distribution of n values, corrected for the fraction of the molecular beam that is overlapped by the laser beam (including its radial intensity dependence), and multiplied by the fraction of the embedded NO_2 molecules that absorb a photon. Note that absorption of the second, third, etc. photons takes place with a higher He_n temperature and the NO_2 not necessarily in its ground state, and results in the evaporation of most of the helium. The resulting lineshapes may differ from those of one-photon excitation, i.e., they are expected to be slightly narrower than for the one-photon case.

Two additional observations argue against $A^2B_2 \leftarrow X^2A_1$ saturation playing an important role. First, saturated transitions would yield comparable intensities for all lines. This is not what is observed; there is an order of magnitude difference between the strong and weak lines in the spectrum shown in Fig. 2. Second, we have recorded a linear fluence dependence of the depletion signal, as shown in Fig. 3. Thus, it is concluded that the large widths are not the result of $A^2B_2 \leftarrow X^2A_1$ saturation. Broadening due to excited state absorption has been reported for gas phase NO_2 [30]. Again, we argue that the large observed widths cannot be attributed solely to this effect, because $\sigma_{abs}\Phi$ values of $\sim 10^4$ would be required.

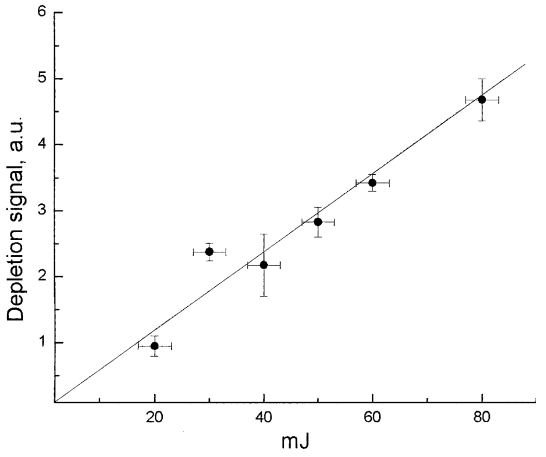

Fig. 3. The depletion signal versus laser fluence can be fitted with a straight line.

Transitions originating from the lowest few rotational levels are contained in a narrow band of frequencies for each vibronic transition. For example, the rotational widths for a number of molecules embedded in He_n (SF_6, OCS, NCCCH, propyne, trifluoropropyne, *tert*-butyl-acetylene, etc.) are <1 cm^{-1} [4,6,11,31]. Only $\Delta K = \pm 1$ transitions with large A rotational constants display large widths [32]. Thus, we believe that rotations do not account for the large widths reported here. Finally, we note that inhomogeneous broadening [27] is insignificant for the cluster sizes and widths reported here.

4.2. The He–NO_2 binary complex

In 1976, Smalley et al. [33] recorded spectra of the He–NO_2 binary complex, and noted that the

frequencies were blue-shifted by approximately 1.5 cm^{-1} relative to those of uncomplexed NO_2 for all of the vibronic bands examined. In addition, widths of approximately 0.8 cm^{-1} (due to dissociation of the complex) were noted for all of the He–NO_2 bands examined.

The origin of these constancies can now be understood as being due to the quantum chaotic nature of the vibronic eigenstates. The number of helium atoms attached to the NO_2 chromophore does not affect this conclusion. It is reasonable to assume that the first shell of He atoms around the NO_2 increases the shifts and widths, and in this sense our results are in accord with this earlier work, though the two sets of experiments were carried out under quite different conditions.

4.3. Mechanism and model

The vibrational relaxation of polyatomic molecules in the regime of regular intramolecular dynamics is known to be mode-specific. Likewise, the predissociation of weakly bound complexes is also known to be mode-specific. The work presented here deals with vibronic levels that each contain numerous combinations of vibrational modes. The fact that the widths and shifts do not vary significantly from one level to the next is consistent with the levels having little mode specific character. Though the origin of this propensity is conceptually straightforward, we cannot yet predict the magnitudes of the widths and shifts, nor their distributions, i.e., dispersions about their mean values.

In bulk liquid helium at 0.37 K, the superfluid fraction is $\rho_s/[\rho_n + \rho_s] = 0.99995$ [34]. Likewise, in 0.37 K He_n droplets having $\langle n \rangle = 9000$, there will be little normal fluid. With an embedded dopant, there is a boundary between the helium atoms adjacent to the dopant and the surrounding superfluid. The relaxation of NO_2 vibronic levels on a picosecond timescale involves mainly the helium atoms adjacent to the NO_2. This follows from the fact that picosecond relaxation times are too short for an excitation to appear in the superfluid. Namely, the NO_2–superfluid distance is ~ 5 Å, which is too large to be accessed in a picosecond, given that the speed of sound in helium is 200 m s^{-1}. Thus, relaxation creates particle-like excitations of the helium atoms that lie immediately adjacent to the NO_2. This is akin to predissociation of a van der Waals complex. The number of lower NO_2 levels thus created, as well as the overall relaxation mechanism as the NO_2 returns to its ground state, are unknown, but will hopefully be figured out in due course.

The proposed model enables some predictions to be made: (i) Photoinitiated unimolecular reactions will be quenched near their gas phase thresholds, because reaction rates must be at least comparable to deactivation rates if there is to be appreciable reaction. (ii) With NO_2, spectra will show (congested) structure at energies up to 25 000 cm^{-1} (for gas phase NO_2, $D_0 = 25128.5\ cm^{-1}$ [35]). (iii) Unlike the gas phase, as D_0 is approached from below, the molecular phase space will not increase along the NO_2 reaction coordinate, because a 'helium blockade' will deny access to the large-r region of the molecular phase space.

Acknowledgements

This research has been supported by the US National Science Foundation, PHY9876991. The authors have benefitted greatly from discussions with Andrey Vilesov, as well as the loan of a turbomolecular pump and a mass spectrometer.

References

[1] J.P. Toennies, A.F. Vilesov, Annu. Rev. Phys. Chem. 49 (1998) 1.
[2] K. Nauta, R.E. Miller, Phys. Rev. Lett. 82 (1999) 4480.
[3] J.H. Reho, J. Higgins, M. Nooijen, K.K. Lehmann, G. Scoles, J. Chem. Phys. 115 (2001) 10265.
[4] M. Hartmann, R.E. Miller, J.P. Toennies, A.F. Vilesov, Phys. Rev. Lett. 75 (1995) 1566.
[5] M. Hartmann, F. Mielke, J.P. Toennies, A.F. Vilesov, Phys. Rev. Lett. 76 (1996) 4560.
[6] S. Grebenev, J.P. Toennies, A.F. Vilesov, Science 279 (1998) 2083.
[7] E. Lugovoj, J.P. Toennies, A.F. Vilesov, J. Chem. Phys. 112 (2000) 8217.
[8] A. Bartelt, J.D. Close, F. Federman, N. Quaas, J.P. Toennies, Phys. Rev. Lett. 77 (1996) 3525.
[9] J.P. Toennies, A.F. Vilesov, K.B. Whaley, Phys. Today (2001) 31.

[10] K.B. Whaley (Ed.), J. Chem. Phys., 115, 2001, special issue on Helium Nanodroplets: A Novel Medium for Chemistry, Physics.
[11] C. Callegari, A. Conjusteau, I. Reinhard, K.K. Lehmann, G. Scoles, J. Chem. Phys. 113 (2000) 10535.
[12] C. Callegari, K.K. Lehmann, R. Schmied, G. Scoles, J. Chem. Phys. 115 (2001) 10090.
[13] K. Nauta, R.E. Miller, J. Chem. Phys. 111 (1999) 3426.
[14] F. Stienkemeier, A.F. Vilesov, J. Chem. Phys. 115 (2001) 10119.
[15] M. Hartmann, A. Lindinger, J.P. Toennies, A.F. Vilesov, J. Phys. Chem. 105 (2001) 6369.
[16] M. Hartmann, A. Lindinger, J.P. Toennies, A.F. Vilesov, Chem. Phys. 239 (1998) 139.
[17] S. Grebenev, M. Havenith, F. Madeja, J.P. Toennies, A.F. Vilesov, J. Chem. Phys. 113 (2000) 9060.
[18] A. Slenczka, B. Dick, M. Hartmann, J.P. Toennies, J. Chem. Phys. 115 (2001) 10199.
[19] A. Delon, R. Jost, M. Lombardi, J. Chem. Phys. 95 (1991) 5701.
[20] A. Delon, R. Jost, J. Chem. Phys. 114 (2001) 331.
[21] B. Kirmse, A. Delon, R. Jost, J. Chem. Phys. 108 (1998) 6638.
[22] R. Georges, A. Delon, R. Jost, J. Chem. Phys. 103 (1995) 1732.
[23] E.S. Medvedev, V.I. Osherov, Radiationless Transitions in Polyatomic Molecules, Springer, Berlin, 1995.
[24] M.L. Mehta, Random Matrices, Academic Press, London, 1991.
[25] M. Lewerenz, B. Schilling, J.P. Toennies, Chem. Phys. Lett. 206 (1993) 381.
[26] J. Davidson, C. Cantrell, A. McDaniel, R. Shetter, S. Madronich, J. Calvert, J. Geophys. Res. 93 (1988) 7105.
[27] X. Zhu, A. Nur, P. Misra, J. Quant. Spectrosc. Radiat. Transfer 52 (1994) 167.
[28] L. Radziemski, R. Solarz, J. Paisner, Laser Spectroscopy its Applications, Marcel Dekker, New York, 1987.
[29] W. Demtröder, Laser Spectroscopy, Springer, Berlin, 1998.
[30] L. Bigio, E.R. Grant, J. Chem. Phys. 83 (1985) 5361.
[31] K. Nauta, D. Moore, R.E. Miller, J. Chem. Soc., Faraday Discuss. 113 (1999) 261.
[32] K. Nauta, R.E. Miller, J. Chem. Phys. 113 (2000) 10158.
[33] R. Smalley, L. Wharton, D. Levy, J. Chem. Phys. 66 (1977) 2750.
[34] S.V. Sciver, Helium Cryogenics, Plenum Press, New York, London, 1986.
[35] R. Jost, J. Nygard, A. Pasinski, A. Delon, Phys. Rev. Lett. 78 (1997) 3093.